Capacitance-voltage characteristics of organic light-emitting diodes varying the cathode metal: Implications for interfacial states

Germà Garcia-Belmonte,[1,*] Henk J. Bolink,[2] and Juan Bisquert[1]
[1]*Departament de Física, Universitat Jaume I, E-12071 Castelló, Spain*
[2]*Institut de Ciència Molecular, Universitat de València, Polígon La Coma s/n, E-46980, Paterna, València, Spain*
(Received 4 May 2006; revised manuscript received 11 October 2006; published 13 February 2007)

Capacitance-voltage (*C-V*) characteristics of organic light-emitting diodes based on a polyphenylene-vinylene have been measured by means of impedance spectroscopy. The effect of the metallic cathode (Au, Ag, Al, Mg, and Ba) was analyzed in the low-frequency region (2 Hz) of the capacitive response. The *C-V* curves collapse into a single pattern in the low bias region, and exhibit a dependence on the cathode work function showing a crossover from positive to negative (inductive) values. The voltage corresponding to the onset of the inductive behavior shifts toward higher bias as the cathode work function increases. Simulations based on an electron-injection model result in agreement with the observed *C-V* characteristics. From the comparison between the predicted and the experimentally observed data an estimation of the energetics of the metal-organic interface could be given. First, an interfacial state located ~0.2 eV above the metal Fermi level appears independently of the metallic cathode. Second, the existence of a dipole layer with interface slope $S=-0.43$ is deduced which enhances relatively the electron injection for large work function metals. In the case of a Ba cathode, the electron barrier determining carrier injection is due to the interface states.

DOI: 10.1103/PhysRevB.75.085316 PACS number(s): 78.66.Qn, 68.35.Fx, 73.61.Ph, 78.60.Fi

I. INTRODUCTION

Interfaces between metals and organic semiconductors constitute a determining part of organic electronics.[1] A fundamental knowledge of the mechanisms underlying charge carrier injection from a metal into an organic semiconductor is essential to design efficient devices. For instance, the issue of reducing the contact series resistance in organic photovoltaic cells and thin-film transistors[2] is critical to improve power conversion and achieve better transistor performance. In the specific case of organic light-emitting diodes (OLEDs), a framework able to predict the injection of charge carriers (particularly electrons) at interfaces between metals and organic semiconductors remains elusive despite the important amount of experimental data and proposed theoretical approaches that are available.[3–8] Since the maximum difference in work function between the anode (usually indium tin oxide) and the metallic cathode is about 2 V, it is generally assumed that the cathode contact may exhibit non-Ohmic features.[9]

Charge-carrier injection at metal-organic interfaces has been analyzed in terms of the diffusion-limited thermionic emission.[10] This approach has been improved by considering the injection into an energetically disordered organic solid as a sequential process in which carriers hop from the metal Fermi level to localized states, exhibiting Gaussian energy disorder, close to the interface.[3,11] Subsequent hops allow carriers to penetrate into the bulk of the organic material and escape from the potential well formed by the superposition of the applied field and the image force in the vicinity of the interface. In this view, the first molecular layer close to the metal strongly experiences the effect of the image potential so as to approximate the molecular energy levels to the metal Fermi level. For electrical fields of the order of 3×10^5 V/cm, typical values of the dielectric constant ($\varepsilon=2-3$) and room temperature, the potential-well top may be reached at a distance from the metallic contact of 10–20 Å, comparable to the size of a few molecular layers.[5]

In addition to the previously explained view, the injection properties of metal-organic interfaces are believed to depend on the properties of a thin organic layer contacting the metal.[12–16] The presence of states within the band gap, due to either a large density of bulk impurities, or interfacial states, will tend to reduce the ability of the organic semiconductor Fermi level E_F to move. The Schottky-Mott limit[17] (absence of interfacial states), which permits the Fermi level to move freely within the gap, is rarely observed in real metal-organic interfaces. A region of net space charge will occur at the interface resulting in an interface dipole. In the limiting case of a high density of interfacial states it is even possible to pin the Fermi level to the position of these states. A useful parameter accounting for this effect is the interface slope[18]

$$S=\frac{dE_F}{d\phi_m}. \tag{1}$$

Here ϕ_m stands for the metal work function. For the Fermi level pinning one obtains $S=0$; and the Schottky-Mott limit results in $S=-1$.

The surface dipole layer formed at the interface, which offsets the vacuum levels of the metal and the organic semiconductor, is able to produce a lowering of the energy levels in the first layers as large as 1 eV. The interface dipole may be either positive (electron injection improved) or negative (hole injection improved). The interface slope S gives the dependence of the energetic offset caused by the formed dipole layer Δ_{dip} with the metal work function. Electronic states of organic layers neighboring the metallic contact are accessible by using ultraviolet (UPS) and inverse (IPS) photoelectron spectroscopies.[17,19,20] Another, related, effect is the formation of new metal-organic states by chemical bonding of the organic molecules at the interface. The specific role of

such interfacial states has been considered in developing injection models based on charge hopping out of interfacial sites whose energy distribution is broadened by the local disorder in the interfacial dipole field.[7,21]

It is also well known that metal-on-organic and organic-on-metal depositions are not completely equivalent. The former deposition technique is confirmed to produce broader interfaces due to in-diffusion of thermally excited metal atoms. In line with this, the asymmetry in the performance of metal/Alq_3/metal devices has been attributed to the formation of oxide layers in one of the interfaces.[17] Similar effects have also been proposed in relation with a chemical oxidation of the metal. UPS analysis revealed in the specific case of Ba/polyphenylenevinylene (PPV) interface a barrier for electron injection of about 0.4 eV built independently of processing conditions by formation of a BaO layer.[22]

The lowest unoccupied (LUMO) and highest occupied (HOMO) molecular orbitals are known to be distributed in energy with a standard deviation of $\sigma_b \approx 0.1$ eV for bulk materials.[23] In case of interfacial layers σ_i is expected to differ from the bulk value. Charge-injection models based on carrier hopping proposed so far make specific assumptions about the energetic disorder of the electronic levels. Some theoretical simulations and analytical models simply treat the energetic disorder of the interfacial molecular layer as that of the bulk material, $\sigma_i \approx \sigma_b$.[3] Here, the first carrier hop is regarded to be the most energetically costly step. Other approaches assume a broadening of the disorder $\sigma_i > \sigma_b$ and see the interfacial molecular level manifold in equilibrium with the metal Fermi level as an electron reservoir.[7] The limiting step is then the hop from the interfacial layer into the bulk distribution. Although the effect of the energetic disorder at the first layers near the metallic contact has been posed into question very recently,[24] there seems to exist a widely accepted consensus insofar as the net shift (lowering) of the molecular energy levels near the contact caused by polarization.

The above discussed injection models were specifically developed with the aim of accounting for static (J-V) characteristics. However, it is widely recognized that crucial and useful device knowledge may be extracted by using some type of kinetic measuring technique, such as impedance spectroscopy (IS). For instance, ac capacitance measurements have been widely applied to determine organic bulk properties such as the carrier mobility variation with the applied voltage.[25–27] When nonohmic contacts govern the charge injection process, IS becomes an important, complementary source of information. Recently we have proposed[28] a kinetic model of electron injection able to account for the commonly observed features of the low-frequency capacitance exhibited by OLEDs. This model considers the particular energetics of the thin molecular layer near the contact, and sees the electron injection as a two-step hopping. The first step involves a hop from the metal Fermi level to interfacial states; and the second step involves a hop from these interfacial states to the bulk. In order to make the model formally simple and mathematically treatable, we explicitly disregarded the effect of the energetic disorder. At least for the interfacial layer, the option of neglecting energetic disorder is in agreement with recent calculations that states $\sigma_i \ll \sigma_b$.[24] Therefore, it becomes feasible to explore the variation of the excess capacitance observed at low frequencies (with respect to the high-frequency geometrical capacitance C_0), and compare them with experimental data. It is well known that OLEDs can exhibit either positive or negative values of the low-frequency capacitance depending on the experimental conditions.[28–30] In addition of interfacial approaches,[28] other views have been proposed that link the excess capacitance with a purely bulk mechanism,[31] which depends on the total stored minority carrier charge.[32,33]

This work deals specifically with the effect of the cathode metal on the low-frequency capacitance of OLEDs under variation of the applied voltage. We used a series of metallic contacts (Au, Al, Ag, Mg, and Ba), which allowed us to vary the metal work function over an energy range of 2.5 eV, while keeping the rest of the device unaltered. As we will show, the excess capacitance exhibits a very coherent pattern with the applied voltage (C-V characteristics). At a certain applied voltage V_c, the capacitance changes sign and becomes negative. This crossover potential, which marks the onset of net electron injection and coincides with the turn on of the light emission, is observed to shift towards higher voltages as the cathode-metal work function increases. The injection model we proposed is able to account for the observed correlation between V_c and the cathode work function. The paper is structured as follows. First, a brief description of the OLED preparation technique is outlined. Second, experimental data on the variation of the low-frequency capacitance versus applied bias for different cathode metals is provided. The analysis of the injection-model implications on the energetics of the metal-organic interfaces finishes this study.

II. EXPERIMENTAL RESULTS

PPV copolymer, "super yellow" (SY) prepared by Merck OLED Materials GMBH, is used as the light emitting polymer (LEP).[34] Different device layouts were investigated in this study, double- and single-carrier devices, using a 200 nm [polyethylenethioxythiophene:polystyrenesulfonic acid (PEDOT:PSS)] hole injection layer, either an 80 or an 150 nm thick SY layer which was covered with a 10 nm thick layer of different metals: barium, magnesium, silver, aluminum and gold. An additional 100 nm thick Al layer was evaporated on top of the cathode metal different from Al, to protect the lower work function metals and serve as an optical mirror. Details on device preparation were published elsewere.[28] J-V characteristics and impedance spectra were collected using an AutoLab PGSTAT30 equipment (Fig. 1). An oscillating amplitude of 10 mV was added to the dc bias voltage using frequencies within the range of 1 MHz down to 1 Hz. Capacitance spectra were obtained from the impedance Z as $C = \mathrm{Re}(1/i\omega Z)$, where $i = \sqrt{-1}$ and ω is the angular frequency of the ac perturbation.

Devices with Au as the cathode metal exhibited no emission within the voltage window employed as expected for the energy difference between the Au work function (5.1 eV) and the LUMO level of SY ($\sim$2.9 eV). By examining Fig. 2, one can observe the main features of the capacitance spectra

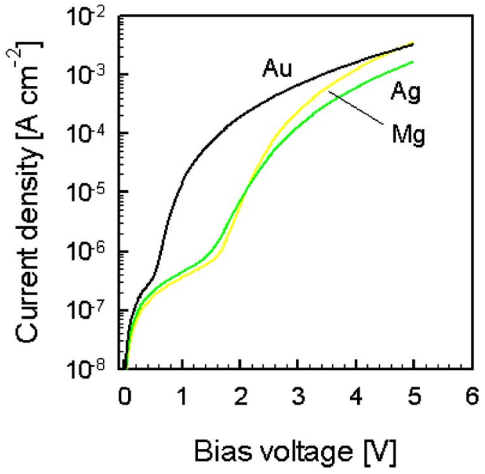

FIG. 1. (Color online) Example of J-V characteristics of OLEDs with structures ITO/PEDOT:PSS/SY/Au (a hole-only device), ITO/PEDOT:PSS/SY/Mg, and ITO/PEDOT:PSS/SY/Ag (double-carrier) devices.

for double- and single-carrier devices. Both types of devices exhibit a plateau in the capacitance at intermediate and high frequencies, which is determined by the dielectric capacitance of the sample (C_0 geometric capacitance). The response for a device with an Au cathode (a hole-only device) [Fig. 2(a)] rises above C_0 as the frequency decreases. A similar capacitance response is observed for the device with an Al cathode (double-carrier device) [Fig. 2(b)]. At higher bias, however, the response changes to an inductive behavior, clearly visible as the negative values reached by the capacitance at low frequencies.

Figure 3 summarizes the C-V characteristics normalized to the geometrical capacitance. The values plotted were obtained from the capacitance spectra at a very low frequency (2 Hz). For all cathodes the capacitance spectra are nearly voltage-independent at low voltages (<1 V) [Fig. 3(a)]. The capacitance increases smoothly as the applied voltage increases. Interesting is that at the potential where light emission starts, a negative contribution to the capacitance appears evolving to a minimum at increasing bias. The hole-only devices did not show the inductive response, indicating that the negative capacitance is related to the injection of electrons from the cathode to the device.

Two points should be noted when observing Fig. 3(a). First, all C-V curves are nearly identical at low bias (0–2 V). Second, at a certain applied voltage V_c, the capacitance sign changes from positive to negative values (inductive response). Importantly, for potentials below V_c all capacitive responses exhibit the same pattern: the C-V curves practically collapse to that obtained from the device having the Au cathode. This would indicate that the mechanism responsible for the capacitance increment at low bias is independent of the type of cathode contact. In the case of large work function metals (Al and Ag) a wide variation in the crossover voltage V_c is observed [Fig. 3(b)]. Nevertheless, there is a rather good correlation between V_c and the cathode-metal work function, which results in $V_c=(1.17+0.43\phi_m)$ V. This implies that the low-frequency capacitive

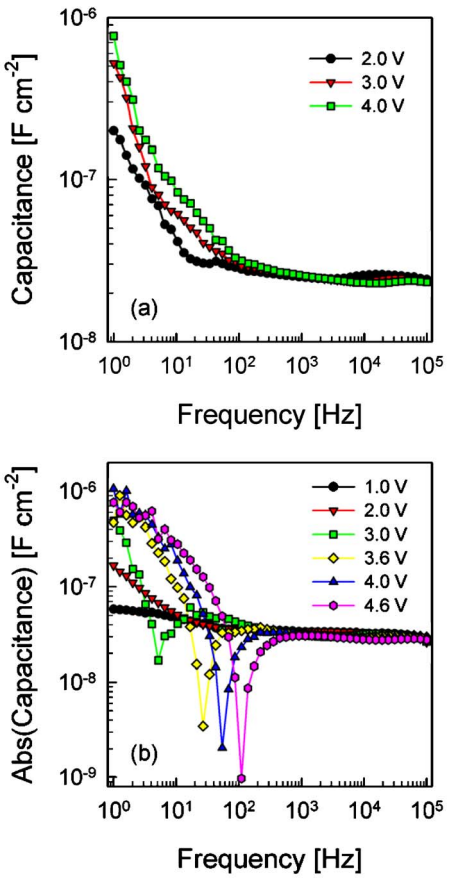

FIG. 2. (Color online) Example of capacitance spectra of OLEDs with structures (a) ITO/PEDOT:PSS/SY/Au (a hole-only device) and (b) ITO/PEDOT:PSS/SY/Al (a double-carrier device). The hole-only devices did not exhibit inductive responses (capacitance always shows positive values).

behavior has its origin in an electronic mechanism at the cathode. If one tries to remove the effect of the built-in potential by plotting C vs $V-V_{BI}$, the responses simply do not collapse into a single pattern in the capacitance raising part. Whereas the built-in potential plays a determining role in establishing the current onset, it does not seem to influence the capacitive response. This is presumably caused by holes injected from the PEDOT:PSS layer into the SY layer, which then form the dominant charge carriers because of the ohmic character of the anode contact.

Standard models accounting for the capacitance spectra of hole-only, space-charge limited systems predict a low-frequency value equal to $\frac{3}{4}C_0$. Excess capacitances as those observed in our experiments ($\sim 20C_0$) were explained either in terms of a frequency-dependent mobility in combination with a distribution in transit time,[25] or by evoking bulk trap states.[27] Our approach is then seen as an alternative explanation relying on interface mechanisms. Importantly, the simulations reported in Ref. 31, which are able to yield negative capacitance values for double-carrier devices, assumed Ohmic contacts or small ($\leqslant 0.2$ eV) effective barrier height for carrier injection from the metal Fermi level into the polymer transport level. For higher work function metals (Ag and Al) an additional potential must be applied in order to

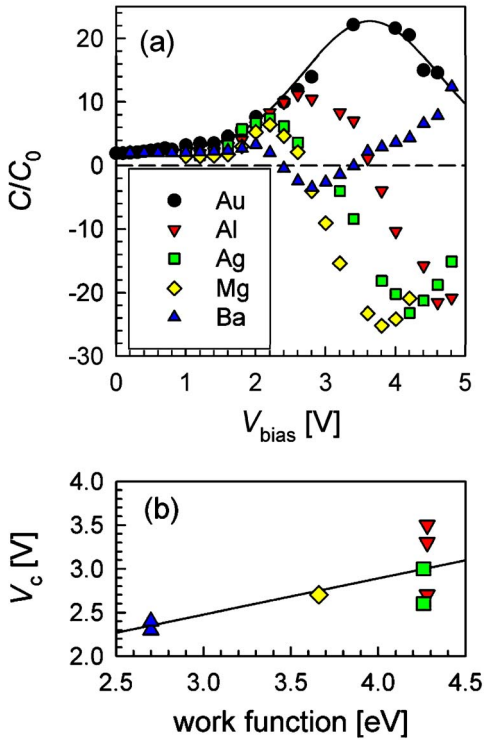

FIG. 3. (Color online) (a) Normalized capacitance with respect to the geometrical capacitance C_0 for different cathode metals. C is directly obtained from the capacitance spectra at a frequency of 2 Hz. The solid line represents a Gaussian-function fit for the Au-based devices, from which a density of states of $N_I=4\times10^{12}$ cm^{-2} is calculated. (b) Dependence of the crossover voltage V_c on the cathode-metal work function ϕ_m taken from Ref. 37. Solid line corresponds to the linear fit $V_c=(1.17+0.43\phi_m)$ V.

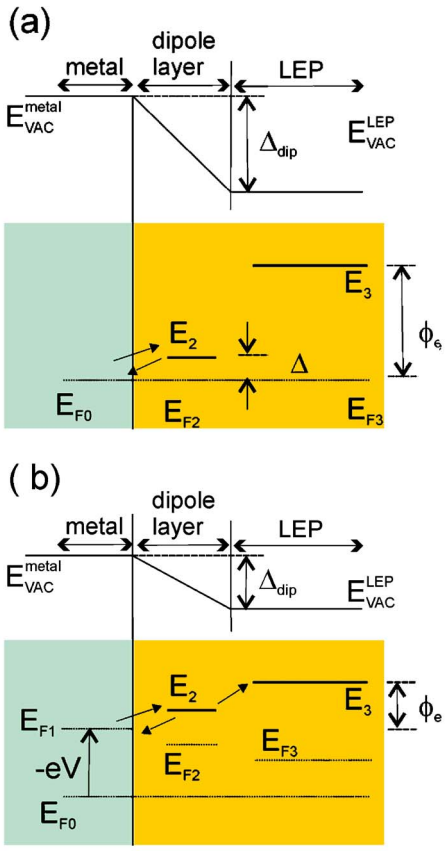

FIG. 4. (Color online) Scheme of the electron injection processes at the metal-organic interface in equilibrium (a) and under negative bias V (b) showing the vacuum level across the interface Δ_{dip}, the Fermi levels and site energies for (1) cathode metal, (2) interface state, and (3) LUMO bulk transport states in the light-emitting polymer. The total electron barrier ϕ_e and the relative position of the interface state with respect to the metal Fermi level Δ are drawn.

achieve sufficient electron injection and then it is expected some type of correlation between the negative capacitance onset and the metal work function (or built-in potential). Nevertheless, a shift of the whole C-V characteristics would be expected assuming a bulk origin if the cathode metal were changed. As noted above, C-V curves shown in Fig. 3(a) collapse into a single pattern in the capacitance raising part with no potential shift. Moreover, all C-V curves belong to the same family of responses at low bias. C-V collapse (in the raising part of the characteristics) is then a distinctive behavior of the low-frequency capacitive response, hardly understandable by assuming a bulk effect. This fact suggests the occurrence of interfacial mechanisms linked with charge injection processes as responsible for the reported capacitive behavior.

III. DISCUSSION

A. Electron injection model

In order to account for our experimental observations, a brief outline of the injection model recently proposed[28] is needed. Figure 4 illustrates the different hopping events governing the electron injection indicated by arrows. Electrons are first injected into intermediate states in the interfacial layer with energy E_2 and density N_I per area at a rate Γ_{12}, and then hop into the bulk transport states with energy E_3 and total density N_B per volume, at a rate Γ_{23}. The corresponding reverse hopping processes consist on the return to the metal cathode from the intermediate states (Γ_{21}) and from the LUMO to the intermediate states (Γ_{32}). A key point of this model is the fractional occupancy of the intermediate state θ, and the electron density in bulk LUMO states, n. The latter is determined by the bulk Fermi level E_{F3} as $n=N_B F(E_3,E_{F3})$, where F is the Fermi-Dirac distribution $F(E,E_F)=\{1+\exp[(E-E_F)/k_BT]\}^{-1}$. Here k_B is Boltzmann's constant and T the absolute temperature. It will be assumed that the LUMO is far from saturated, $n\ll N_B$, so that $F(E_3,E_{F3})$ reduces to the Boltzmann distribution. It is useful to define a quasi-Fermi level E_{F2} for the intermediate state as $\theta=F(E_2,E_{F2})$.

It is assumed that the jump rate from an occupied localized state i to an empty state j is written following a symmetric transition as suggested for polaron hopping in organic systems:[35]

$$\Gamma_{ij} = \nu_{ij} \exp\left(-\frac{E_j - E_i}{2k_B T}\right) \tag{2}$$

The jump prefactors ν_{ij} set the timescale for each hopping process. The net carrier flux between pairs of states are given by

$$\upsilon_{12} = k_{12} N_I \left\{ (1-\theta)\exp\left(-\frac{E_2 - E_{F1}}{2k_B T}\right) - \theta \exp\left(\frac{E_2 - E_{F1}}{2k_B T}\right) \right\}, \tag{3}$$

$$\upsilon_{23} = k_{23} N_B N_I \left\{ \theta \exp\left(\frac{E_2 - E_3}{2k_B T}\right) - \frac{n}{N_B}(1-\theta)\exp\left(-\frac{E_2 - E_3}{2k_B T}\right) \right\}. \tag{4}$$

The kinetic constants k_{ij} relate to the jump prefactors as $k_{12}=\nu_{12}$ and $k_{23}=\nu_{23}/N_B$. The steady state, electron current density $j(V)$ is determined by the equations $j=e\upsilon_{12}=e\upsilon_{23}$, which can be solved numerically.

When a negative potential is applied to the cathode, the metal Fermi level increases with respect to the equilibrium Fermi level E_{F0} as $E_{F1}=E_{F0}-eV$ where e is the elementary charge. For describing the displacement of the intermediate energy level we assume a linear shift with respect to the initial value E_2^0 as $E_2=E_2^0+\gamma_1(E_{F1}-E_{F0})$, where γ_1 (with $0<\gamma_1\leqslant 1$) is a constant parameter that determines whether the energy E_2 accompanies E_{F1} ($\gamma_1\approx 1$) or remains close to E_3 ($\gamma_1\approx 0$). The increasing negative potential at the cathode induces an electron flow towards the bulk. The ac response of the injection process is described by the impedance function $Z_c=\Delta V/\Delta I$ where ΔV and ΔI denote a small signal periodic perturbation of the cathode potential and current, imposed over a steady state. The current injected at the contact is given by $\Delta I=eA\Delta\upsilon_{12}$ where A is the area. The kinetic model can be linearized with respect to ΔV and $\Delta\theta$ and solved for Z_c eliminating $\Delta\theta$.[28] The capacitance $C_c=\mathrm{Re}(Y_c/i\omega)$ can be calculated accordingly. We demonstrated[28] that the low-frequency (equilibrium) capacitance is proportional to the variation of the interfacial state occupancy with the bias voltage $C_c=eN_I\,\mathrm{d}\theta/\mathrm{d}V$. Simulations based on the described model have been published recently.[36]

B. Comparison with experimental *C-V* characteristics

The general trends observed for the *C-V* characteristics of different cathodes can be understood by varying only one parameter in the injection-model introduced above while fixing the rest of the parameters. This parameter, the level E_3, which represents the energetic distance between the cathode-metal work function (Fermi level in equilibrium) and the LUMO energy in the organic bulk, was varied accordingly yielding the occupancy and low-frequency capacitance limit shown in Fig. 5. In the simulation the energy level E_2 practically accompanies the change of the metal Fermi level with applied bias ($\gamma_1=0.95$). The energy level E_3 corresponds to the total electron potential barrier

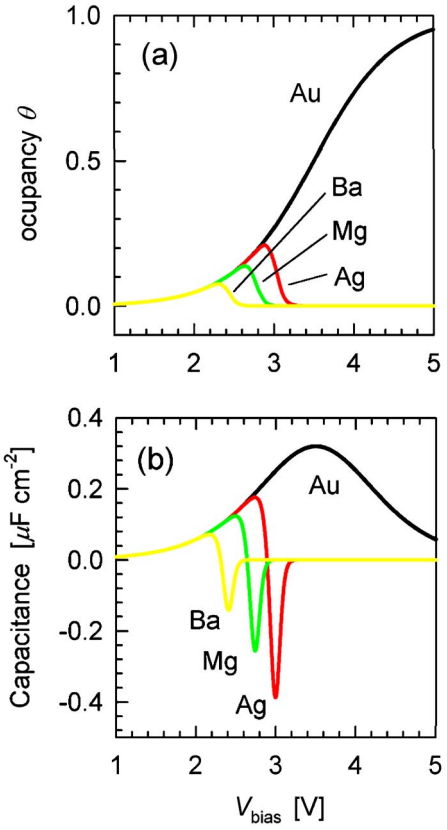

FIG. 5. (Color online) Occupancy of the interfacial state (a) and capacitance (b) as a function of bias voltage resulting from the model simulations of electron injection with the following values for the fixed parameters: $N_I=4\times10^{12}$ cm^{-2}, $N_B=10^{20}$ cm^{-3}, $E_{F0}=0.0$ eV, $E_2^0=0.2$ eV, $\nu_{12}=10^{13}$ s^{-1}, $\nu_{23}=10^{-9}$ s^{-1}, and $\gamma_1=0.95$. The energy level E_3 which corresponds to the total electron potential barrier $\phi_e=(\phi_m-\Delta_{\mathrm{dip}})-\mathrm{LUMO}$ was varied as 0.0 eV (Ba), 0.33 eV (Mg), 0.58 eV (Ag) in accordance with the interface dipole energy offset. To show the full occupancy case with Au as cathode metal, E_3 was situated at 4.0 eV.

$$\phi_e = (\phi_m - \Delta_{\mathrm{dip}}) - \mathrm{LUMO}. \tag{5}$$

The simulation shows that the negative capacitance response shifts towards lower bias for smaller work function metals. This is in good agreement with the experimental *C-V* characteristics of Fig. 3. Additionally, all curves collapse into a single curve in the raising part of the response at low bias. Moreover, it results from the simulation that the voltage V_c, corresponding to the crossover from positive to negative capacitance, shifts towards higher voltages linearly with ϕ_e and unity constant proportionality. In case of hole-only devices (Au as the cathode metal) the model predicts an almost full occupancy of the intermediate states to be reached within the applied voltage window used. For this case it is then possible to estimate the interfacial state density directly by integration of the *C-V* curve. The Gaussian-function fit is represented by the solid line in Fig. 3(a), from which a density of states of $N_I=4\times10^{12}$ cm^{-2} is calculated. As the capacitance was read at 2 Hz, this density of states does not correspond to a true equilibrium value. We should alert that the calculated inter-

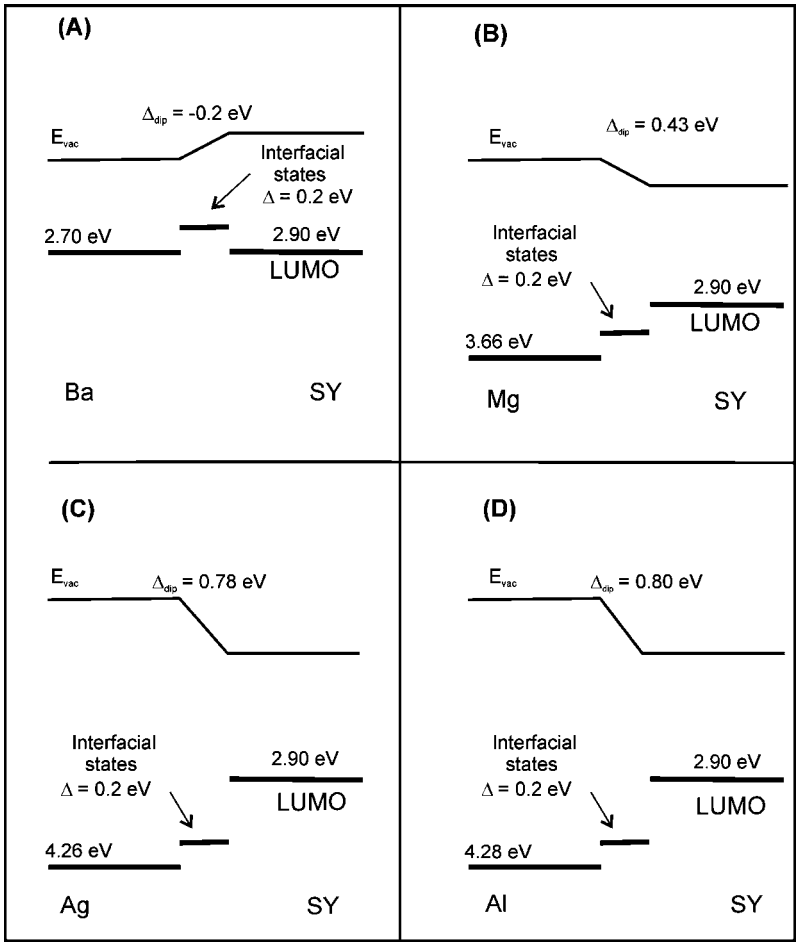

FIG. 6. Energetics of the metal-organic interface for different cathode metals (Ba, Mg, Ag and Al), as derived from the injection-model. The LUMO level in case of Ba has been aligned with the metal Fermi level, assuming that the electron barrier is determined by the position of the interface state. The dipole layer offsets the vacuum energy according to the slope parameter $S=-0.43$. The interface state is located $\Delta=0.2$ eV above the metal Fermi level.

facial density of sates is likely an underestimation of the real value. However, the order of magnitude obtained lies within typical values reported in the literature.[7]

Accordingly, we used this density value in the rest of the simulation while keeping fixed the interfacial energy level in equilibrium at $\Delta=E_2^0-E_{F0}=0.2$ eV. By assuming a constant level for these states, the model fixes the interfacial sites at a certain energetic distance from the metal Fermi level. In the simulations the hopping rate constants were fixed at $\nu_{12}=10^{13}$ s^{-1} and $\nu_{23}=10^{-9}$ s^{-1}. The rate prefactor for the metal-interfacial layer hop ν_{12} was chosen to be equal to the usual attempt-to-escape frequency of electronic transitions in the range of $10^{12}-10^{13}$ s^{-1}. Note that in order to reproduce the *C-V* responses of Fig. 5, the second rate prefactor ν_{23} should be lower than the first one by many orders of magnitude. As pointed out by Wolf *et al.*,[11] the effective injection rate into a layer of hopping sites must be lower than predicted by the Richardson-Schottky mechanism, an indeed values of the Richardson coefficient smaller by several orders of magnitude than that reported for inorganic semiconductors were found.[6] The origin for this experimental observation was related to the special dynamics of the injected carriers trying to escape from the potential well built by the image force. Analytical models describe the process in terms of a diffusion-assisted Onsager-type mechanism in an energetically dispersed landscape.[3] The slowing down effect for the second transition observed in our simulations thus entails that charge carriers take some time to escape from the interfacial layer out to bulk states. It should be also noted that electron injection occurs in conditions out of equilibrium so as to expect rate prefactors which may differ from usual values in equilibrium conditions. In addition, in assuming polaronic instead of Miller-Abrahams transition probabilities in Eq. (2) the effective hopping rate is enhanced in case of downward hop so as to reach reasonable current densities at working potentials.

The injection-model presented, although based on simple assumptions, is able to capture the essential features of the injection dynamics. As stated previously, the model explicitly disregards the effect of the site energy dispersion. Moreover, the transition between the interfacial layer up to bulk polymer states is oversimplified as a single jump. The reason for this was obviously to keep only essential ingredients into the formulation, which allows us to calculate ac responses. By comparing Fig. 3(a) and Fig. 5, one can realize that the negative capacitance variation with the bias voltage is observed to be smoother for the experimental data than that obtained in the simulation. We can suggest that the smoothing behavior may be an effect of the energetic disorder of the organic states that is not considered in the injection-model used. Work is in progress to improve our analysis by exploring the effect of Gaussian density distributions.

As experimentally observed, the voltage V_c is roughly proportional to the cathode work function as $V_c \propto 0.43\phi_m$. The simulation, however, yields a variation of the form $V_c \propto \phi_e$. The difference between the experimentally observed and the model-predicted dependencies are a result of the di-

pole layer Δ_{dip}. In the devices studied in this work it turns out that the dipole offset enhances electron injection by reducing the barrier. Such a reduction is larger for increasing cathode work functions. Recalling now the interface slope parameter S defined in Eq. (1), one readily obtains that $V_c \propto -S\phi_m$ because S includes the energy level modification caused by the interface dipole. We are therefore able to get an estimation of the interface slope which results in a value for $S=-0.43$.

Using the differences between the experimental C-V characteristics (Fig. 3) and those obtained from simulations, it is feasible to derive the energy level scheme of the metal/polymer for the series of different cathode materials used as depicted in Fig. 6. For low work function metals such as Ba, the expected potential barrier ϕ_e must be negative or nearly zero but the interfacial state E_2^0, situated above the metal Fermi level, introduces an additional potential barrier which inhibits electron injection to some extent. In case of metals with a larger work function the effect of the interfacial state is less dramatic since the value of the total potential barrier is solely determined by the energetic difference between the bulk LUMO and the metal Fermi level.

By considering the value obtained for the interface slope, one would have expected the observation of inductive responses for Au at much lower bias. One possible explanation for this could be a quite different dipole effect in case of large work function metals such as Au. However, a kinetic rather than equilibrium explanation is more likely. For Au as cathode metal, the rate prefactors, especially ν_{23}, may differ by orders of magnitude from those assumed for the rest of the metallic contacts. In the simulations of Fig. 5, E_3 was situated at 4.0 eV in order to reproduce the full occupancy case with Au as cathode metal. It should be noted that devices using Au as cathode exhibit light emission at large bias voltages, generally above 8 V.

Apart from the net effect of the dipole layer, the simulation performed on the injection-model predicts a fixed position of the interfacial state E_2^0, independent of the metal work function. E_2^0 is located $\Delta \sim 0.2$ eV above the metal Fermi level. Only by keeping this interfacial level fixed, the collapse of the C-V curves in a single response at low bias is obtained. This can be interpreted as a sort of Fermi level pinning for such interfacial state. The constancy in the E_2^0 level suggests that some type of chemical modification occurs at the metal-organic layer. Due to the fact that the interface state accompanies the metal work function we are inclined to think about the formation of a metal oxide layer, as proposed by other authors[22] in case of Ba/PPV interfaces. In practical terms our interpretation would entail that the deposition technique used (metal evaporation on top of the organic layer) unavoidably produces a chemical alteration of the metal-organic interface by the formation of a layer of new entities at the interface (presumably a metal oxide layer). In order to verify the implications derived from the injection model on the energetics of the metal-organic interfaces, the combination of surface analysis techniques and ac electrical measurements will be needed.

IV. CONCLUSIONS

In summary, our kinetic model, based on simple assumptions about charge carrier injection at the device cathode, is able to reproduce the main features of the capacitive response: the exclusively positive capacitance response for hole-only devices, the collapse into a single pattern in the low bias region, and the shift toward lower bias of the inductive behavior for smaller work-function cathodes, in good correlation with experimental C-V curves. The excess capacitance is related to the change of occupancy of the interfacial states. The detailed analysis of the experimentally observed and the predicted C-V curves enables the deduction of the energy levels of the states involved in the charge injection process. An interface state having an energy level 0.2 eV above the metal Fermi level is observed independently of the metal cathode used. Additionally, the analysis revealed the presence of a dipole layer at the interface with an interface slope $S=-0.43$ which enhances the probability of electron injection for higher work function metals.

ACKNOWLEDGMENTS

We would like to thank Merck OLED Materials for the supply of the light-emitting polymer SY. The work was supported by Generalitat Valenciana and Fundació Caixa Castelló Bancaixa under Project No. P1 1B2005-12. H.B. acknowledges the support of the Program "Ramon y Cajal" of the Spanish Ministry of Education and Science.

*Electronic address: garciag@uji.es

[1] Y. Shen, A. R. Hosseini, M. H. Wong, and G. G. Malliaras, ChemPhysChem **5**, 16 (2004).
[2] L. Bürgi, T. J. Richards, R. H. Friend, and H. Sirringhaus, J. Appl. Phys. **94**, 6129 (2003).
[3] V. I. Arkhipov, E. V. Emelianova, Y. H. Tak, and H. Bässler, J. Appl. Phys. **84**, 848 (1998).
[4] V. I. Arkhipov, U. Wolf, and H. Bässler, Phys. Rev. B **59**, 7514 (1999).
[5] J. C. Scott and G. G. Malliaras, Chem. Phys. Lett. **299**, 115 (1999).
[6] S. Barth, U. Wolf, H. Bässler, P. Müller, H. Riel, H. Vestweber, P. F. Seidler, and W. Riess, Phys. Rev. B **60**, 8791 (1999).
[7] M. A. Baldo and S. R. Forrest, Phys. Rev. B **64**, 085201 (2001).
[8] W. R. Silveira and J. A. Marohn, Phys. Rev. Lett. **93**, 116104 (2004).
[9] V. I. Arkhipov and H. Bässler, Appl. Phys. Lett. **77**, 2758 (2000).
[10] P. R. Emtage and J. J. O'Dwyer, Phys. Rev. Lett. **16**, 356 (1966).
[11] U. Wolf, V. I. Arkhipov, and H. Bässler, Phys. Rev. B **59**, 7507 (1999).
[12] S. Narioka, H. Ishii, D. Yoshimura, M. Sei, Y. Ouchi, K. Seki, S. Hasegawa, T. Miyazaki, Y. Harima, and K. Yamashita, Appl. Phys. Lett. **67**, 1899 (1995).
[13] C. Shen and A. Kahn, Org. Electron. **2**, 89 (2001).

[14] J. C. Scott, J. Vac. Sci. Technol. A **21**, 521 (2003).
[15] J. X. Tang, C. S. Lee, T. S. Lee, and Y. B. Xu, Chem. Phys. Lett. **396**, 92 (2004).
[16] F. Amy, C. Chan, and A. Kahn, Org. Electron. **6**, 85 (2005).
[17] A. Kahn, N. Koch, and W. Gao, J. Polym. Sci., Part B: Polym. Phys. **41**, 2529 (2003).
[18] I. G. Hill, D. Milliron, J. Schwartz, and A. Kahn, Appl. Surf. Sci. **166**, 354 (2000).
[19] X. Crispin, V. Geskin, A. Crispin, J. Cornil, R. Lazzaroni, W. R. Salaneck, and J.-L. Bredas, J. Am. Chem. Soc. **124**, 8131 (2002).
[20] H. Peisert, M. Knupfer, T. Schwieger, J. M. Auerhammer, M. S. Golden, and J. Fink, J. Appl. Phys. **91**, 4872 (2002).
[21] B. N. Limketkai and M. A. Baldo, Phys. Rev. B **71**, 085207 (2005).
[22] A. Crispin, A. Jonsson, M. Fahlman, and W. R. Salaneck, J. Chem. Phys. **115**, 5252 (2001).
[23] J. Bisquert, G. Garcia-Belmonte, and J. García-Cañadas, J. Chem. Phys. **120**, 6726 (2004).
[24] S. V. Novikov and G. G. Malliaras, Phys. Rev. B **73**, 033308 (2006).
[25] H. C. F. Martens, H. B. Brom, and P. W. M. Blom, Phys. Rev. B **60**, R8489 (1999).
[26] H. C. F. Martens, W. F. Pasveer, H. B. Brom, J. N. Huiberts, and P. W. M. Blom, Phys. Rev. B **63**, 125328 (2001).
[27] H. H. P. Gommans, M. Kemerink, G. G. Andersson, and R. M. T. Pijper, Phys. Rev. B **69**, 155216 (2004).
[28] J. Bisquert, G. Garcia-Belmonte, A. Pitarch, and H. J. Bolink, Chem. Phys. Lett. **422**, 184 (2006).
[29] L. S. C. Pingree, B. J. Scott, M. T. Russell, T. J. Marks, and M. C. Hersam, Appl. Phys. Lett. **86**, 073509 (2005).
[30] V. Shrotriya and Y. Yang, J. Appl. Phys. **97**, 054504 (2005).
[31] H. H. P. Gommans, M. Kemerink, and R. A. J. Janssen, Phys. Rev. B **72**, 235204 (2005).
[32] M. A. Green and J. Shewchun, Solid-State Electron. **16**, 1141 (1973).
[33] S. E. Laux and K. Hess, IEEE Trans. Electron Devices **46**, 396 (1999).
[34] H. Becker, H. Spreitzer, W. Kreuder, E. Kluge, H. Schenk, I. Parker, and Y. Cao, Adv. Mater. (Weinheim, Ger.) **12**, 42 (2000).
[35] D. H. Dunlap, P. E. Parris, and V. M. Kenkre, Phys. Rev. Lett. **77**, 542 (1996).
[36] J. Bisquert, G. Garcia-Belmonte, J. M. Montero, and H. J. Bolink, Proc. SPIE **6192**, 619210 (2006).
[37] H. B. Michaelson, J. Appl. Phys. **48**, 4729 (1977).